Int J Earth Sci (Geol Rundsch)
DOI 10.1007/s00531-012-0790-3

ORIGINAL PAPER

Investigating the kinematics of local thrust sheet rotation in the limb of an orocline: a paleomagnetic and structural analysis of the Esla tectonic unit, Cantabrian–Asturian Arc, NW Iberia

Arlo Brandon Weil · Gabriel Gutiérrez-Alonso · David Wicks

Received: 3 November 2011 / Accepted: 8 May 2012

Abstract The Esla tectonic unit lies along the southern boundary of the Cantabrian–Asturian Arc, a highly curved foreland fold-thrust belt that was deformed during the final amalgamation of the Pangea supercontinent. Previous structural and paleomagnetic analyses of the Cantabrian–Asturian Arc suggest a two-stage tectonic history in which an originally linear belt was bent into its present configuration, creating an orocline. The Esla tectonic unit is a particularly complex region due to the interaction of rotating thrust sheets from the southern limb of the arc and the southward-directed thrusts of the Picos de Europa tectonic domain during late-stage north–south shortening and oroclinal bending. These structural interactions resulted in intense modification of early-phase thin-skinned tectonic structures that were previously affected by a deeper out-of-sequence antiformal stack that passively deformed the early thrust stack. A total of 75 paleomagnetic sites were collected from the Portilla and Santa Lucia formations, two carbonate passive-margin reef platform units from the middle Devonian. Similar to other regions of the Cantabrian–Asturian Arc, Esla Unit samples carry a secondary remanent magnetization that was acquired after initial thrusting and folding of Variscan deformation in the late Carboniferous. Protracted deformation during late-stage oroclinal bending caused reactivation of existing thrust sheets that include the Esla and younger Corniero and Valbuena thrusts. When combined with existing structural data and interpretations, these data indicate that the present-day sinuosity of the Esla Unit is the consequence of both secondary rotation of originally linear features in the western Esla exposures (e.g., frontal thrusts), and secondary modification and tightening of originally curvilinear features in the eastern Esla exposures (e.g., hanging-wall lateral/oblique ramps). Differences in structural style between the Esla and other tectonic units of the arc highlight the complex kinematics of oroclinal bending, which at the orogen-scale buckled an originally linear, north–south (in present-day coordinates) trending Cantabrian–Asturian thrust belt during the final stages of Pangea amalgamation.

Keywords Orocline · Cantabrian–Asturian Arc · Esla Unit · Variscan · Paleomagnetism · Thrust-belt kinematics · Rotations · Iberia

A. B. Weil (✉) · D. Wicks
Department of Geology, Bryn Mawr College, Bryn Mawr, PA 19010, USA
e-mail: aweil@brynmawr.edu

G. Gutiérrez-Alonso
Departamento de Geología, Universidad de Salamanca, 37008 Salamanca, Spain

Introduction

All orogenic systems have some degree of map-scale curvature, whether it is at the mountain belt scale or thrust sheet scale, there is inevitably an observable variation in structural trend. This observation has stimulated fundamental research into how the progression of an orogen's deformation history, and specifically its kinematic evolution, results in curvature (e.g., Marshak 1988, 2004; Pérez-Estaún et al. 1988; Marshak et al. 1992; Allerton 1998; Hindle and Burkhard 1999; Weil and Sussman 2004; Van der Voo 2004; Weil et al. 2010a, b). Previous efforts to explain orogenic curvature (Weil and Sussman 2004) have described three basic categories: primary arcs, where curvature is created without any rotations around vertical axes; progressive arcs, where there is a partial contribution to the

Published online: 04 June 2012

overall geometry from local vertical-axis rotations as deformation progresses; and oroclines, where curvature is associated with a secondary deformation phase that rotated an initially linear orogen around a vertical axis to its present-day orientation. It is clear from the varying degrees of vertical-axis rotation in each of these models that to truly understand how a particular orogenic system becomes curved; it is necessary to quantify the amount and spatial distribution of rotations in combination with classic translation and strain data (Yonkee and Weil 2010).

Although vertical-axis rotations are known to be an integral part of a region's deformation history, they are often difficult to quantify unless using paleomagnetic techniques (e.g., Irving and Opdyke 1965; Kotasek and Krs 1965; Grubbs and Van der Voo 1976; Channell et al. 1978; Van der Voo and Channell 1980; Schwartz and Van der Voo 1984; Kent and Opdyke 1985; Eldredge et al. 1985; Lowrie and Hirt 1986; Miller and Kent 1986a, b; Eldredge and Van der Voo 1988; Kent 1988; Muttoni et al. 1998, 2000; Weil et al. 2000, 2001; Weil 2006; Pueyo et al. 2007). Local rotations are determined when stable remanence directions are measured and compared to known regional paleomagnetic reference declinations obtained from undeformed and stable areas proximal to the deformed region (e.g., Demarest 1983). Unlike conventional structural geology techniques, paleomagnetism provides a stable external reference frame (the Earth's spin axis) for restoring crustal blocks back to their initial orientation by quantifying both near-field and far-field vertical-axis rotations (MacDonald 1980; McCaig and McClelland 1992; Allerton 1998; Pueyo et al. 2003, 2004). In many cases, paleomagnetic analyses can help in resolving competing kinematic models by accurately constraining the spatial, and sometimes temporal, distribution of rotations. In this paper, we will test existing structural models for a classic imbricate-duplex thrust system in the southern arm of the Cantabrian–Asturian Arc (CAA) using a densely sampled paleomagnetic dataset from multiple thrust sheets. When combined with existing structural data and interpretations, these data improve our understanding of the deformation path in this region with emphasis on how individual thrust systems accommodate secondary rotation due to changes in the regional stress field and the development of oroclinal bending.

The CAA is the un-metamorphosed foreland fold-thrust belt of the Western European Variscan Belt (WEVB) (Pérez-Estaún et al. 1991) (Fig. 1) and the core of the larger Iberian-Armorican Arc (IAA). Its 180° of arc curvature has inspired a variety of tectonic models that explain how the orogen acquired its current geometry; however, little consensus exists between the different models. While there is general agreement that two separate deformation phases occurred, various models have considered that curvature was caused by the following factors: dextral transpression around a Gondwana indentor (e.g., Ribeiro et al. 2007); a change in thrust transport direction over time as a result of a continuously changing stress field (e.g., Pérez-Estaún et al. 1988); or large lithospheric-scale dextral shearing (Martínez-Catalán 2011); whereas more recent models explain the curvature by secondary oroclinal bending (e.g., Weil et al. 2000; Weil 2006). To resolve these conflicting hypotheses, acquisition of new quantitative vertical-axis rotation data is needed to provide limits for testing the viability of a given model to various tectonic units in the CAA.

The Fold-and-Nappe belt represents the outermost tectonic units of the CAA and is comprised of the Aramo, Somiedo-Correcillas, Valsurbio, Sobia-Bodón, and Esla Units of Fig. 1. More open folds dominate the northern zone of the Fold-and-Nappe belt, whereas along the southern curve of the arc, the deformation style changes to a thrust dominated imbricate system (Julivert 1971; Julivert and Marcos 1973; Julivert and Arboleya 1984; Alonso et al. 2009). Calcite twin, fracture, and paleomagnetic data, along with recent three-dimensional fold analysis, suggest that at least some portions of the southern and northern limbs of the arc have undergone upwards of 90° of rotation, with respect to the hinge zone, subsequent to early folding and faulting (Weil et al. 2000, 2001; Kollmeier et al. 2000; Pastor-Galán et al. 2011, 2012).

The Esla Unit (Fig. 2) is located at the east-central edge of the southern CAA limb and is a particularly complex tectonic unit due to its multiphased deformation history and the interaction of thin-skinned thrust nappes, deeper out-of-sequence duplex systems, and thrust reactivation all in close proximity (Arboleya 1981; Alonso 1987). Structural modification was further complicated by re-activation of the Porma fault (Fig. 2), which developed from a tear fault related to thrust-parallel transport in the early stages of deformation, then switched to a reverse fault during strain field rotation (Alonso 1987; Alonso et al. 2009). The reactivation of the Porma fault is therefore integral to explaining the sinuous thrust traces observed in the present-day exposure of the Esla Unit.

Geometric and kinematic models have been proposed for the contribution of reactivated Esla Unit thrust sheets to folds in the Stephanian synorogenic sequences (Alonso 1989) that unconformably overlie the Esla Unit. However, these models cannot quantify or verify potential vertical-axis rotations, due to the restrictive nature of using a two-dimensional deformation perspective (i.e., classic 2-D cross-section restoration). Previous paleomagnetic studies in the CAA have been centered on large-scale, polydeformed tectonic structures in both the Fold-and-Nappe region of the outer CAA as well as the Ponga Unit, which lies north of the Esla Unit (Ries et al. 1980; Bonhommet

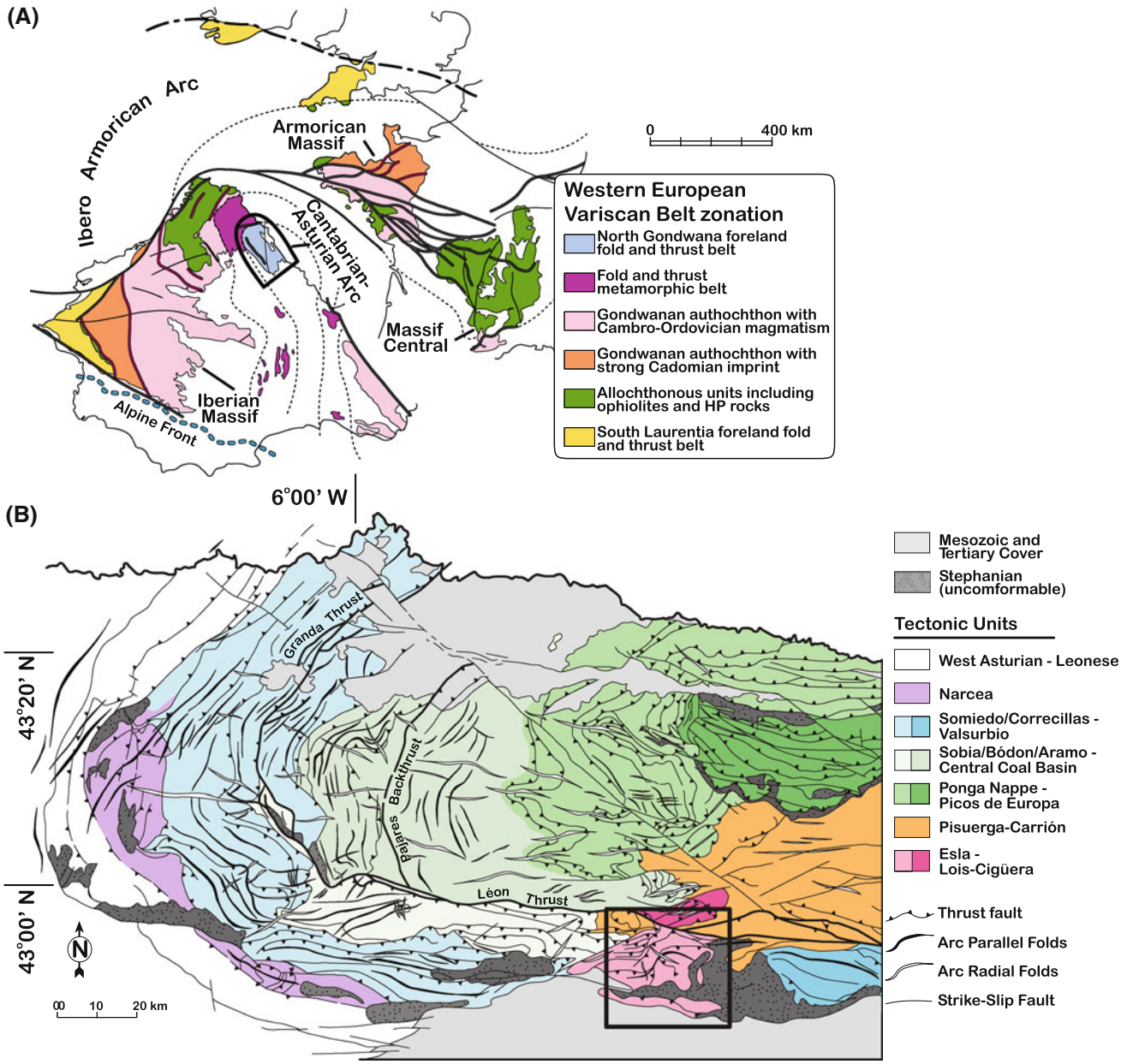

Fig. 1 **a** Simplified tectonostratigraphic zonation of the Western European Variscan Belt (WEVB) in southwestern Europe (figure modified from Martínez-Catalán et al. 2007; Franke 2000). Location of Cantabrian–Asturian Arc is highlighted with a black box in the core of the larger Iberian Armorican Arc. **b** Structure/tectonic map of the Cantabrian–Asturian Arc, highlighting the geometry of major thrusts and the orientation of arc-parallel and arc-perpendicular folds. Tectonic unit divisions modified from Alonso et al. (2009). *Black box* surrounds the Esla Unit shown in more detail in Fig. 2

et al. 1981; Perroud 1986; Hirt et al. 1992; Parés et al. 1994; Stewart 1995a; Van der Voo et al. 1997; Weil et al. 2000, 2001; Weil 2006), but as yet there are no detailed paleomagnetic studies in the eastern portion of the southern CAA limb.

Complicating any paleomagnetic study is the characterization of the remanent magnetism in the sampled rocks. Unfortunately, many rock units are not useful for paleomagnetic analysis either because of the inadequate mineralogy/granulometry for carrying a stable ancient remanence, or because regional remagnetization caused by protracted tectono-thermal or fluid exposure has modified and/or overprinted any meaningful signal (Van der Voo and Channell 1980). Previous work in the CAA (Parés et al. 1994; Stewart 1995a, b; Van der Voo et al. 1997; Weil et al. 2000, 2001; Weil and Van der Voo 2002a) shows that there are at least two ancient magnetic components preserved in the remanence of Paleozoic carbonates.

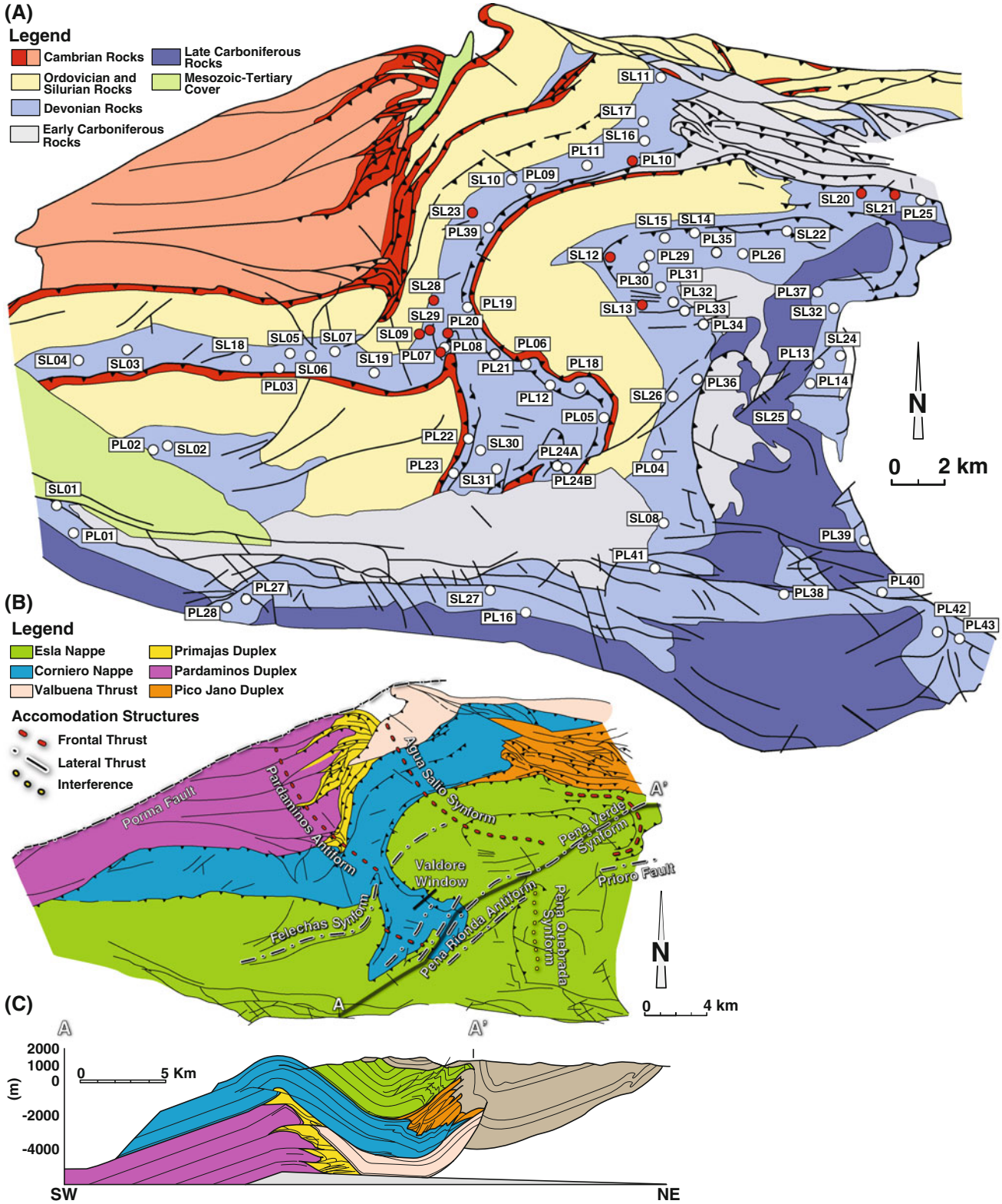

Fig. 2 **a** Geological sketch map of the Esla Unit, highlighting the site locations (*white circles*). *Red-filled symbols* denote those sites that did not produce reliable paleomagnetic data. **b** Simplified structural map of the Esla Unit, highlighting the different exposed nappes, thrust sheets and duplexes. Main drape-fold structures related to footwall ramps and flats labeled and marked by dashed lines. **c** Geologic section of the nappe-stack in the Esla Unit. Structure map and cross-section modified from Alonso (1987)

However, there is yet a stable primary magnetization confirmed in any pre-Carboniferous rock units within the CAA. The oldest interpreted remagnetization was acquired during initial 'longitudinal' deformation (D1) and is referred to as the 'C' component (Parés et al. 1994). A second remagnetization event is constrained to the time between initial deformation and secondary 'radial' deformation (D2) and is referred to as the 'B' component (Parés et al. 1994; Van der Voo et al. 1997; Weil et al. 2000, 2010a, b). Thus, the C magnetization is established as syn-folding and the B magnetization as post-folding, but both the B and the C magnetizations were acquired prior to D2 radial folding, vertical-axis rotation, and oroclinal bending. The established relationship between secondary magnetization acquisition and deformation allows the paleomagnetic declinations to be used as a reference marker for quantifying subsequent rotation about vertical, inclined, or horizontal axes.

The Esla Unit represents an ideal area for investigating the interaction between thrust sheet displacement and subsequent vertical-axis rotation, two important controls on the overall kinematic history of the CAA foreland, and fold-thrust belts in general. The aim of this study is to better understand the kinematics of the Esla Unit using paleomagnetic and structural data to constrain the late-stage deformational history of the CAA, as well as highlight the utility of detailed paleomagnetic studies in complex structural settings.

Geologic background

The WEVB (Fig. 1) represents the core of the Variscan orogen, which stretches across much of present-day Western and Eastern Europe. The Variscan system represents the eastern extent of the orogeny between Laurentia, Gondwana, Baltica, and several Rheic Ocean microcontinents during the final amalgamation of Pangea (e.g., Matte 1986, 1991; Franke et al. 2005). The WEVB attracts a good deal of attention for its sinuous map pattern. A large portion of the WEVB in northern Iberia was a passive-margin peri-Gondwanan siliciclastic–carbonate platform that was an active depocenter for much of the Paleozoic (García-Alcalde 1995; Aramburu et al. 2002; Wotte 2009). Sedimentation overlapped with orogeny-related tectonism in the Carboniferous and is well preserved today in several unconformable, synorogenic Carboniferous basins scattered throughout the CAA (e.g., Marcos and Pulgar 1982; Colmenero et al. 2008; Keller et al. 2007, 2008).

The CAA (Fig. 1) consists of several tectonic units that have been differentiated based on their lithologies and deformation styles. Some are dominated by folds whereas others are dominated by multiple thrust packages (Julivert 1971; Julivert and Marcos 1973; Julivert and Arboleya 1984; Pérez-Estaún et al. 1988; Alonso et al. 2009). The Esla Unit (Arboleya 1981; Alonso 1987) is made up of three repeated successions of Cambrian through Devonian siliciclastic rocks and carbonates (Fig. 2a), which are stratigraphically and paleogeographically correlated with the westernmost units of the Cantabrian Zone, where most previous paleomagnetic studies have been performed (e.g., Hirt et al. 1992; Stewart 1995a; Van der Voo et al. 1997; Weil et al. 2000). The Esla Unit is composed of several thrust sheets, including the Esla Nappe, which is structurally the highest thrust sheet, the underlying Corniero Nappe, and the lowermost Valbuena thrust sheet (Alonso 1987) (Fig. 2b, c). This thrust stack was later modified by the out-of-sequence emplacement of the Pardaminos antiformal stack and the Primajas duplex. Stephanian synorogenic deposits covered the entire unit and today crop out in the northeastern part of the Esla Unit (Fig. 2).

Samples for this study were collected from the Devonian Portilla and Santa Lucia formations. The entire Devonian succession in the Fold-and-Nappe province and Esla Unit is up to 2,000-m thick and is composed of near-shore deposits, alternating between siliciclastics and carbonates. The Santa Lucía Formation is a 250-m-thick massive limestone with shallower facies toward the core of the CAA. Its age is from Late Emsian to Early Eifelian (Méndez-Bedia 1976). The Portilla Formation is a 60- to 250-m thick massive limestone unit with several biostromal episodes. Its age is Late Givetian to earliest Frasnian (García-López 2002). The distributions of these facies, which in general stratigraphically thicken to the south and to the west, represent a back barrier, to barrier and fore-barrier reef environment near the ancient coastline (De Sitter 1965; Reijers 1980, 1985; Méndez-Bedia et al. 1994; Fernández et al. 1997; Hofmann and Keller 2006).

Early and Middle Devonian times in the WEVB were a relatively quiescent tectonic period, which saw minor crustal extension, regional sedimentation and reef evolution (Keller 1997). This changed in the Late Devonian to an overall compressive regime as Variscan collision initiated (e.g., Santos Zalduegui et al. 1995; Rodríguez et al. 2003). The effects of collision produced a flexural bulge in the Cantabrian Zone that caused a new prograding sedimentation cycle (García-Ramos and Colmenero 1981; Keller et al. 2007, 2008). Subsequent Variscan foreland fold-thrust belt deformation imparted a negligible amount of internal strain (Pastor-Galán et al. 2009) and localized dolomitization in the CAA (Tornos and Saphiro 2000; Gasparrini et al. 2003, 2006). Reviews of the stratigraphy, lithology, basin history, and general structural and tectonic history of the region can be found elsewhere (e.g., Julivert 1971; Julivert and Marcos 1973; Reijers 1980, 1985; Pérez-Estaún et al. 1988; Keller et al. 2008).

Methods

A total of 75 sites in the Portilla and Santa Lucia formations were collected over the summers of 2002, 2003, and 2010, yielding a total of about 750 oriented core samples. Samples were collected using a portable gas powered drill and oriented with a magnetic compass. Bedding planes were measured at every site using a magnetic compass. Portilla Formation sites were preferred due to their better magnetic behavior during demagnetization when compared to the Santa Lucia Formation. Core samples were brought back to the Bryn Mawr College paleomagnetic laboratory and cut into standard 2.54-cm paleomagnetic specimens.

Rock magnetic experiments were carried out on many of the samples to strengthen the understanding of the magnetic minerals that carry magnetism in the Portilla and Santa Lucia formations. Hysteresis properties were measured on 89 specimens using a Princeton Measurements Vibrating Sample Rock Magnetometer (Micro-VSM) and a Princeton Measurements Alternating Gradient Magnetometer converted to a Micro-VSM at the Institute of Rock Magnetism.

Between 6 and 13 paleomagnetic specimens from each site were progressively demagnetized in either an Analytical Service Co. thermal demagnetizer or a D-Tech2000 alternating field (AF) demagnetizer. After measurement of the natural remanent magnetization, thermal demagnetization was run at 50 °C increments up to 200, 40 °C increments up to 280, 30 °C increments up to 400, 25 °C increments up to 500, and 10 °C increments until fully unblocked. Samples subjected to AF treatment were demagnetized at 2, 5, 8, 10, 13, 16 mT, increments of 5 mT from 20 to 40 mT, increments of 20 mT from 40 to 100 mT, and increments of 25 mT from 100 to 200 mT. Magnetic intensity and direction were measured between each demagnetization step using an Agico JR-6a spinner magnetometer in a low-field magnetic cage in the Bryn Mawr College paleomagnetic laboratory, as well as on a 2-G Superconducting Rock Magnetometer (SRM) at the Institute of Rock Magnetism at the University of Minnesota. Remanence directions were calculated from principle component analysis (Kirschvink 1980) of linear demagnetization directions acquired from orthogonal projection plots of vector endpoint diagrams (Zijderveld 1967) using the SuperIAPD software suite.

Results

Hysteresis measurements

Hysteresis measurements were made on both whole specimens and rock chips from each of the 23 sites collected in the summer of 2010. All hysteresis loops were slope corrected to remove any paramagnetic or diamagnetic imprint (Fig. 3). There is a mixture of unsaturated and saturated samples, but the majority of the measured specimens are saturated at very low fields (less than 2.0 T and often less than 1.0 T), suggesting the dominance of a low-coercivity mineral phase such as magnetite. About a third of the samples (32/89) were more resistant to saturation, which represents the minor presence of a higher coercivity phase,

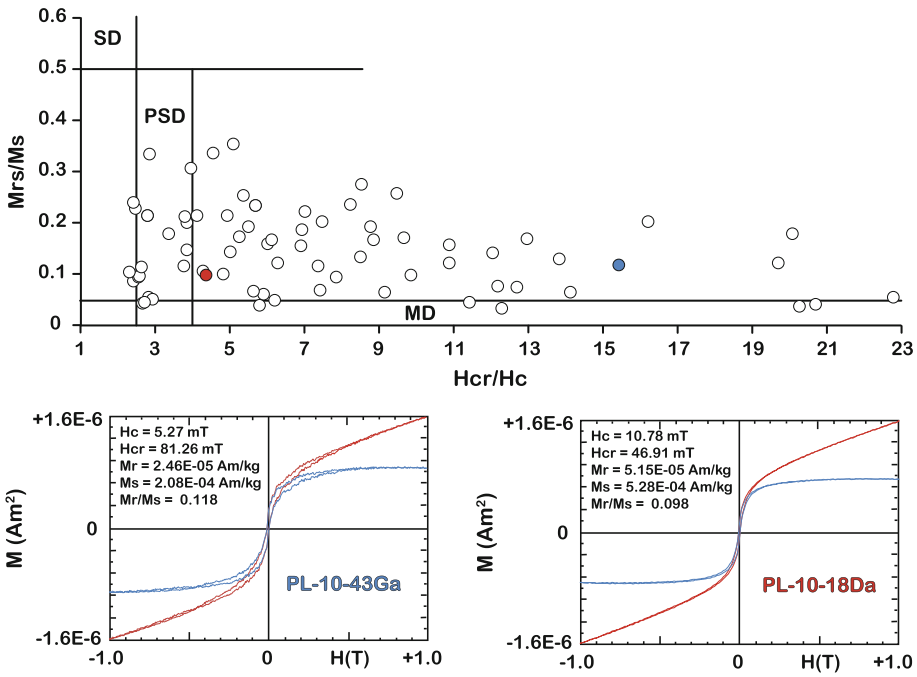

Fig. 3 Hysteresis ratios plotted according to Day et al. (1977) (labeled zones represent: *SD* single domain, *PSD* pseudo-single domain, *MD* multi-domain magnetic particle size). Hc is coercive force, Hcr is remanent coercivity, Mr is isothermal remanent magnetization, and Ms is saturation magnetization. *Red-* and *blue-filled circles* represent the *two hysteresis curves* shown. Typical examples of slope corrected (*blue curves*) hysteresis loops showing wasp-waisting. *Red curves* are uncorrected hysteresis loops, indicating a paramagnetic influence at high field strengths

like hematite. Almost all the hysteresis loops show a typical wasp-waisted shape that is often associated with remagnitized limestones (Jackson et al. 1992; McCabe and Channell 1994; Tauxe et al. 1996; Weil and Van der Voo 2002b) and represents a mixture of single domain (SD) and superparamagnetic (SP) magnetite grains. Detailed rock magnetic behavior of both Santa Lucia and Portilla Formation carbonates can be found in Weil and Van der Voo (2002b).

Paleomagnetism

Measured specimens were demagnetized using both AF and thermal demagnetization procedures since both techniques can be independently used to isolate a stable remanent magnetization (Fig. 4). Out of the 75 sites measured, eleven sites did not provide enough stable specimens (four in the Portilla and seven in the Santa Lucia) to calculate a meaningful site direction using Fisher statistics (Fisher 1953), or had $\alpha 95$ values greater than 15° (Table 1). The majority of the sites preserved a weak low-coercivity overprint that was removed by 150 °C or 8 mT. This is consistent with previous studies in the CAA (Weil 2006; Weil et al. 2010a, b) and is interpreted as a weak viscous overprint of the present-day field in northern Spain ($D = 354°$, $I = 59°$). Sixty-four sites carry a stable characteristic remanent magnetization (ChRM) that typically has a south to easterly declination and a low to moderate inclination (Fig. 5). This magnetization unblocks between 250 and 450–500 °C or 60–100 mT, which is characteristic of other remagnetized Paleozoic carbonates from southwestern Europe (Thominski et al. 1993; McCabe and Channell 1994; Molina-Garza and Zijderveld 1996; Weil and Van der Voo 2002b; Zegers et al. 2003).

Tectonic corrections and fold tests

Similar to previous studies from the CAA (e.g., Stewart 1995a; Van der Voo et al. 1997; Weil et al. 2000, 2001; Weil 2006), most in situ paleomagnetic site mean directions from the Esla Unit lie near the southeastern quadrant (Fig. 5) and have both positive and negative inclinations.

Thrust fault systems and related folds dominate the structural setting of the Esla Unit, which provides several small-scale (decameter wave length) and large-scale (km wave length) folds for constraining relative timing of

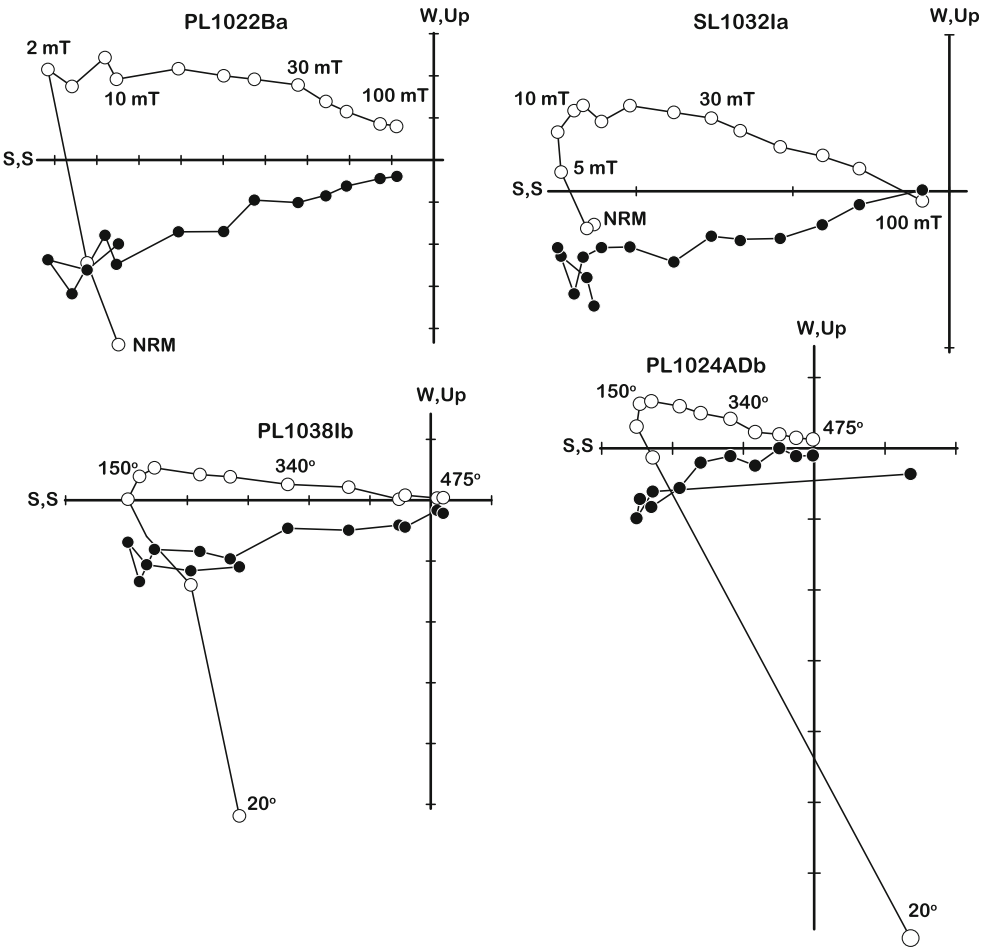

Fig. 4 Representative examples of progressive thermal and alternating field demagnetization behavior of in situ Esla Unit samples using orthogonal demagnetization diagrams (Zijderveld 1967). In each diagram, the endpoint of the magnetization vector is projected onto the *horizontal plane* (*solid circles*) and the *vertical plane* (*open circles*) using, in all cases, the E-W axis as the common projection axis. Demagnetization steps are indicated along data points on the horizontal projection in degrees C for thermal and mT for alternating field demagnetization. Tic marks on both axes are 1.0 mA/m

Table 1 Paleomagnetic and structural site information and statistical parameters for the Esla Unit

Site number	Lat.	Long.	N/No	Strike	Tectonic corrections		In situ site mean			
					Dip Dir.	Dip	Dec	Inc	α95	*k*
Portilla Formation										
PL01	42.8380	−5.2947	10/11	120	210	49	74.4	6.5	10.7	21.3
PL02	42.8537	−5.2703	11/12	115	205	42	135.7	−6.0	8.9	27.4
PL03	42.8728	−5.2355	8/8	87	357	75	160.4	−23.9	11.9	22.7
PL04	42.8539	−5.1236	9/9	5	95	67	169	−5.3	4.2	151.2
PL05	42.8615	−5.1394	11/11	12	102	82	177.2	0.8	6.3	54.2
PL06	42.8732	−5.1622	12/12	314	44	28	169.1	−18.5	5.1	73.2
PL07[b]	42.8778	−5.1862	0/13	19	109	86	–	–	–	–
PL08	42.8778	−5.1862	6/8	154	244	42	166.3	−11.1	12.2	31.1
PL09[a]	42.9079	−5.1618	9/12	80	350	106	119.7	0.6	11.7	20.4
PL10[b]	42.9148	−5.1327	0/13	81	171	90	–	–	–	–
PL11[a]	42.9124	−5.1444	7/9	80	350	118	73	4.4	8.9	46.6
PL12	42.8675	−5.1557	8/12	307	37	31	178.8	−17.4	4.7	142.1
PL13[a]	42.8721	−5.0787	8/9	151	61	95	178.6	−21.4	4.1	185.9
PL14	42.8706	−5.0791	9/9	216	306	66	171.4	−23.2	4.7	122.4
PL-10-16[a]	42.8216	−5.1638	6/9	137	47	102	94.2	−17.1	14.3	29.6
PL-10-17[b]	42.9034	−5.1775	0/12	229	319	66	–	–	–	–
PL-10-18	42.8673	−5.1469	8/8	258	348	37	168.3	−19.5	3.6	234.5
PL-10-19	42.8831	−5.1802	5/8	354	84	50	152.6	−19.2	12.8	36.9
PL-10-20[b]	42.8779	−5.1863	0/8	32	122	79	–	–	–	–
PL-10-21	42.8745	−5.1726	7/8	314	44	28	147.9	7.0	7.4	67.4
PL-10-22	42.8558	−5.1788	7/8	230	320	38	165.7	−17.1	8.0	57.6
PL-10-23	42.8502	−5.1822	8/8	224	314	33	180.3	−8.1	13.5	17.8
PL-10-24A	42.8507	−5.1521	6/7	205	295	19	163	−5.6	10.7	39.9
PL-10-24B	42.8504	−5.1522	6/6	33	123	34	160.9	−4.8	11.9	32.7
PL-10-25	42.8740	−5.0501	7/8	108	198	82	154.4	−4.0	8.5	51.8
PL-10-26[a]	42.8964	−5.1000	6/7	124	34	99	157.7	−2.3	6.1	123.3
PL-10-27	42.8236	−5.2458	8/8	63	153	67	28.6	−7.8	9.1	38.0
PL-10-28	42.8239	−5.2516	8/9	145	235	56	94.5	14.7	5.8	91.4
PL-10-29	42.8939	−5.1278	7/8	321	51	69	167.1	−13.3	10.1	36.71
PL-10-30	42.8912	−5.1285	8/8	324	54	51	170.7	−5.8	8.3	45.9
PL-10-31	42.8874	−5.1242	9/9	313	43	49	174.2	−3.3	8.1	41.6
PL-10-32	42.8843	−5.1205	7/10	322	52	57	181.3	−11.9	15.4	16.2
PL-10-33	42.8821	−5.1179	4/8	337	67	36	155.2	−7.6	13.3	48.5
PL-10-34	42.8807	−5.1168	9/11	334	64	44	170.8	−0.3	12.7	17.5
PL-10-35	42.8966	−5.1064	8/8	289	19	84	149.9	−1.2	9.4	36.0
PL-10-36[a]	42.8681	−5.1145	8/8	354	264	103	170.7	−16.6	7.5	55.5
PL-10-37	42.8860	−5.0799	8/8	204	294	74	177.6	−22.7	7.8	51.2
PL-10-38	42.8205	−5.0880	11/12	80	170	69	167.9	−9.2	5.9	61.3
PL-10-39	42.8319	−5.0622	7/8	149	239	69	136.6	−10	5.6	190.4
PL-10-40	42.8256	−5.0600	7/8	114	204	47	181.2	4.0	5.2	133.7
PL-10-41[a]	42.8299	−5.1300	8/8	89	359	104	166.7	3.3	11.1	25.9
PL-10-42	42.8162	−5.0426	8/8	173	263	33	196	27.6	8.2	46.3
PL-10-43[a]	42.8152	−5.0398	6/6	7	277	124	198.2	28.2	14.7	21.8
Santa Lucia Formation										
SL01	42.8425	−5.2984	9/13	122	212	65	73.3	−11.6	12.6	17.7
SL02	42.8543	−5.2687	9/9	124	214	27	142.2	0.5	9.5	30.0

Table 1 continued

Site number	Lat.	Long.	N/No	Strike	Tectonic corrections		In situ site mean			
					Dip Dir.	Dip	Dec	Inc	α95	*k*
SL03[a]	42.8749	−5.2841	10/12	89	359	128	106.1	−18.5	12.6	15.6
SL04[a]	42.8731	−5.2982	7/7	71	341	122	103.8	−27.2	7.1	73.4
SL05	42.8738	−5.2297	8/10	140	230	65	143.6	3.4	5.8	92.6
SL06[a]	42.8731	−5.2277	9/12	93	363	95	153.5	−4.5	8.5	37.3
SL07[d]	42.8748	−5.2198	9/12	114	204	85	149.8	−14.9	15.0	
SL08[a]	42.8396	−5.1221	10/10	12	282	95	183.8	−5.0	6.3	60.5
SL09[b]	42.8781	−5.1896	0/10	27	117	86	–	–	–	–
SL10[a]	42.9100	−5.1660	11/12	65	335	104	65.6	26.2	12.3	13.8
SL11	42.9318	−5.1207	7/7	95	185	68	139.2	12.8	12.3	24.9
SL12	42.8930	−5.1386	12/13	332	242	61	233.8	−18.3	11.2	16.0
SL13[b]	42.8846	−5.1298	0/6	334	244	43	–	–	–	–
SL14	42.9000	−5.1112	7/13	92	182	87	157.1	−23.6	7.7	61.6
SL15	42.8994	−5.1205	9/12	89	179	71	164	−35.7	7.2	52.1
SL16	42.9184	−5.1269	8/10	277	367	39	76	47.7	6.8	66.6
SL17	42.9194	−5.1270	9/11	108	198	43	112.4	51.9	13.8	14.8
SL18[a]	42.8719	−5.2450	9/9	83	353	115	106.2	−20.5	9.5	30.3
SL19[a]	42.8709	−5.2073	7/9	90	360	94	98.6	5.3	10.4	34.9
SL20[b]	42.9064	−5.0619	0/6	80	170	80	–	–	–	–
SL21[b]	42.9074	−5.0510	0/6	302	32	80	–	–	–	–
SL22[a]	42.8997	−5.0872	7/7	87	357	94	174.1	−15.1	7.2	88.3
SL23[a,b]	42.9049	−5.1781	0/6	39	309	112	–	–	–	–
SL24	42.8741	−5.0731	6/6	190	280	73	183	−24.1	10.8	39.7
SL25	42.8626	−5.0855	6/6	155	245	55	165.5	−14.8	6.7	102.2
SL26[a]	42.8653	−5.1193	6/6	15	285	111	173.4	−20.5	9.3	52.7
SL-10-27	42.8261	−5.1744	6/6	119	209	84	85.9	−2.4	9.4	51.5
SL-10-28[c]	42.8845	−5.1879	7/7	28	118	66	65.4	20.3	24.9	8.17
SL-10-29[b]	42.8781	−5.1894	0/6	16	106	83	–	–	–	–
SL-10-30	42.8539	−5.1754	6/6	234	324	31	170.5	−10.1	9.8	49.7
SL-10-31	42.8500	−5.1710	6/8	241	331	78	177.4	−6.0	13.1	27.0
SL-10-32	42.8840	−5.0763	6/6	204	294	81	178.1	−23.1	8.4	64.2

Lat and Long are site location latitude and longitude in decimal degrees; N/No gives the ratio of samples used in the analysis to samples demagnetized; Strike—in degrees using the right-hand rule; Dip Dir. and Dip in degrees; Dec and Inc are in situ declination and inclination, respectively, in degrees; α95 and k are the statistical parameters associated with the site mean (Fisher 1953)

[a] Designates overturned bedding

[b] Designates a site that could not be used (explained in text)

[c] Designates a site not used due to >15° α95

[d] Designates a site that required great-circle analysis (Hoffman and Day 1978)

magnetization acquisition with respect to deformation (Fig. 6). A total of five fold tests are presented that have statistically significant results at the 95 % confidence interval. Where possible, the parametric bootstrap fold test was used when enough data were available from both limbs of a fold (Tauxe and Watson 1994; Tauxe 1998). For those folds where sites were limited, the classic fold test of McElhinny (1964) was used, as it is impossible to use the parametric bootstrap technique with a small number of sites. In all cases, fold tests were performed on both plunge corrected and in situ paleomagnetic site mean data, and in all cases the fold tests gave similar results, usually with a slight increase in statistical significance after plunge correction.

None of the five fold tests presented have a peek clustering of directions different from 0 to 10 % unfolding (Fig. 7). A fold test of a km-scale fold structure was performed on the combined 11 sites from the Agua Salio Synform (PL26, PL29, PL30, PL31, PL32, PL33, PL34, PL35, SL14, SL15, and SL22) (Fig. 6), a drape fold

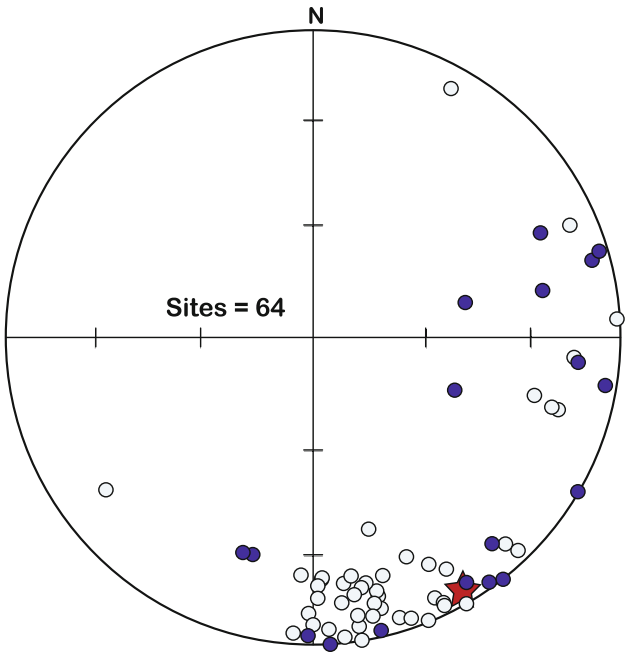

Fig. 5 Equal area projections of paleomagnetic site mean data from the Esla Unit. All site means are plotted in in situ coordinates. Closed (*open*) symbols refer to lower (*upper*) hemisphere projections. Note the large degree of declination scatter away from the expected reference direction (*red star*)

(Butler 1982) associated with hanging-wall deformation over a D1 frontal ramp (Alonso 1987). The axial trace of the Agua Salio Synform trends WNW-ESE. The in situ magnetic declinations trend SSE, are sub-parallel on both limbs of the fold, and have consistent shallow and up inclinations (Fig. 7). Peak clustering occurs between −10 and +8 % unfolding, which coincides with a 'B' component magnetization. A second fold test was performed on 13 sites in the Valdoré Window (PL05, PL06, PL08, PL12, PL18, PL19, PL21, PL22, PL23, PL24a, PL24b, SL30, and SL31) (Fig. 6), where the Corniero Nappe is exposed in an anticlinal fold between the western and eastern limits of the Esla Nappe. The Valdoré Window is associated with the frontal culmination of the Pardaminos antiformal stack, which caused substantial uplift of the Corniero Nappe during its emplacement (Fig. 2c) (Alonso 1989). Similar to the Agua Salio Synform, the in situ magnetic declinations are sub-parallel on both limbs of the exposed folds, with shallow inclinations. Peak clustering occurs between −4 and +25 % unfolding, which coincides with a 'B' component magnetization. A final regional fold tests was done on 10 sites from the Peña Quebrada Synform (SL08, SL24, SL25, SL26, SL32, PL04, PL13, PL25, PL36, and PL37), a sinuous roughly N–S trending drape fold located between

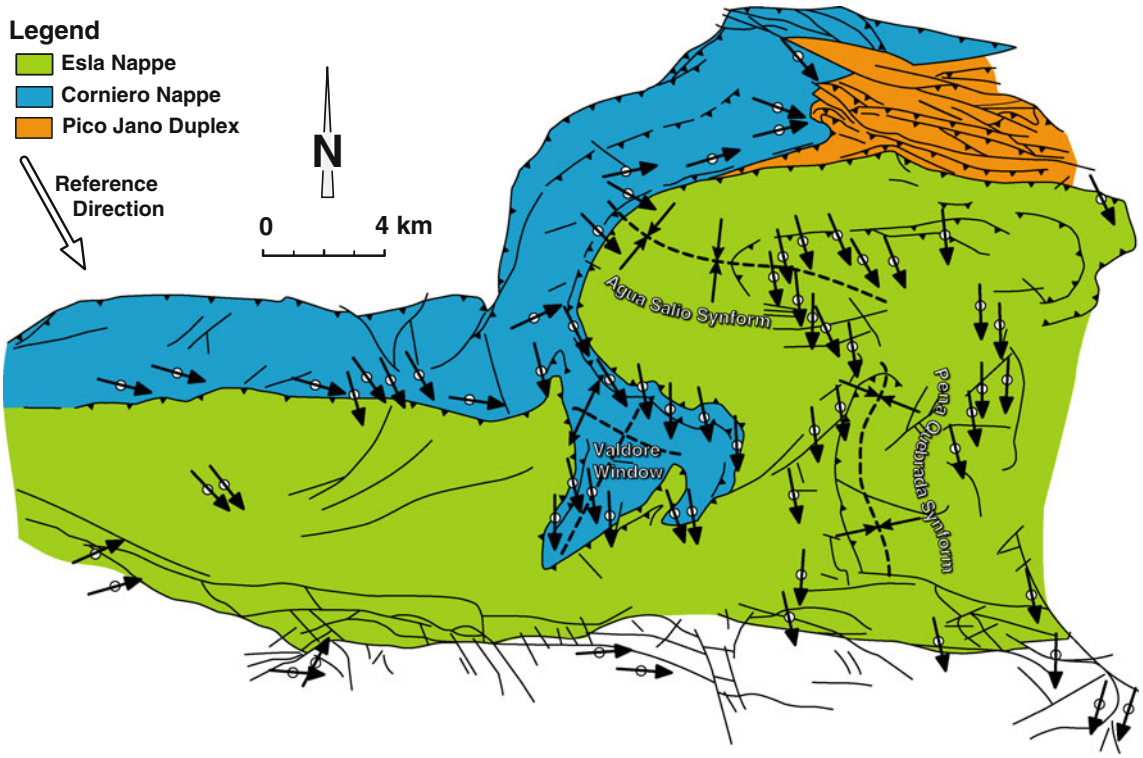

Fig. 6 Structural map of the Esla Unit showing in situ site mean declinations. *White circles* indicate paleomagnetic site locations from this study, and *black arrows* represent the direction of in situ paleomagnetic site mean declinations. Major fold traces used for incremental fold tests are labeled for convenience

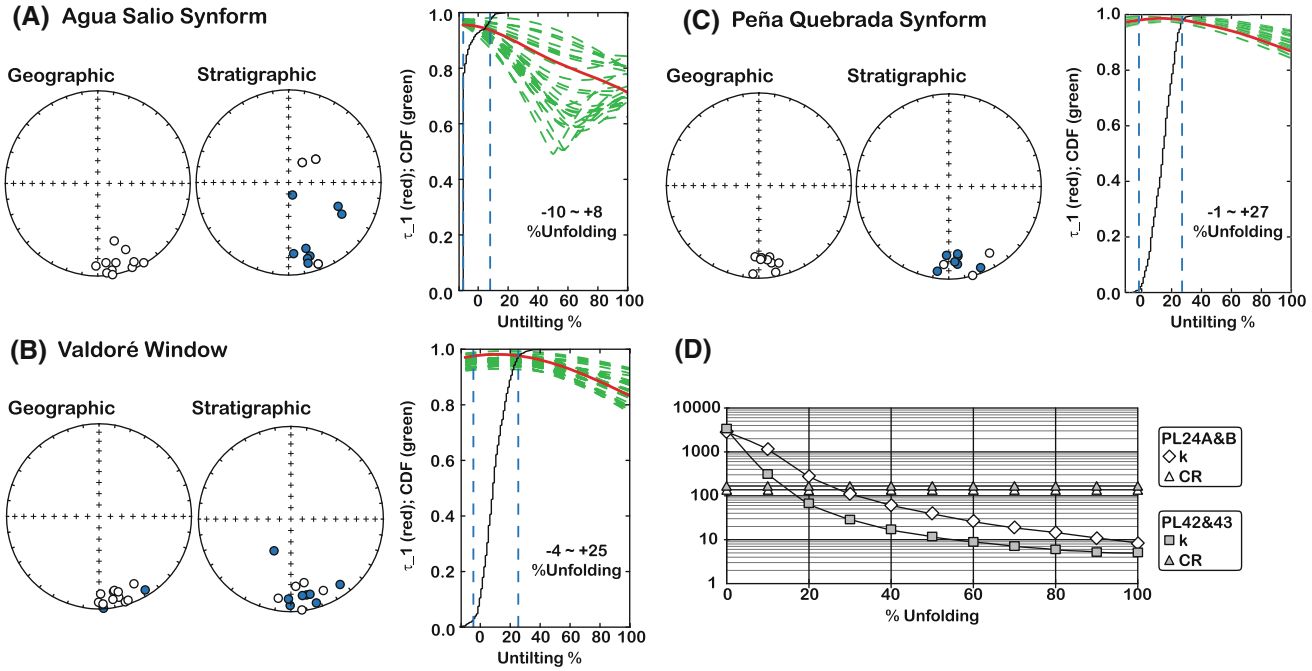

Fig. 7 **a–c** incremental parametric bootstrap fold tests from the Agua Salio Synform, Peña Quebrada Synform and Valdoré Window. The τ-1 parameter represents the largest eigenvalue of the orientation matrices from representative para-datasets (*green dashed lines*). Histogram represents 500 maxima of τ-1 with their respective fraction of maximum given by the *right-hand* side ordinate axis. Calculated 95 % confidence intervals are bracketed by *blue dashed lines*. **d** Two incremental fold tests for decameter-scale folds, plotting the kappa parameter (*open diamond* and *filled square*) and CR values (*open* and *filled triangles*) versus percent unfolding (McElhinny 1964). The CR parameter is the critical ratio above which the kappa value is significant at the 95 % confidence interval. Maximum kappa in both cases is reached at 0 % unfolding

frontal and lateral ramps in the Esla Nappe (Alonso 1987). Once again, in situ magnetic declinations are sub-parallel on both limbs of the exposed folds, with shallow inclinations. Peak clustering occurs between −1 and +27 % unfolding, which further supports a 'B' component magnetization carried by Esla Unit carbonates. Two outcrop-scale folds (sites PL24 and PL24b; sites PL42 and PL43) were sampled and resulted in a peak clustering at 0 % unfolding.

Following the previous work in the Fold-and-Nappe province (Van der Voo et al. 1997; Weil et al. 2000, 2001; Weil 2006), the ChRM identified in the Esla region is interpreted as the late Carboniferous 'B' magnetization. The 'B' component is close to the inferred late Carboniferous reference direction for the stable interior of Iberia (Weil 2006) and is therefore a secondary magnetization that post-dates D1 folding, but precedes the rotations responsible for oroclinal bending (D2) (Weil et al. 2001).

Age assessment of the 'B' magnetizations was initially described in detail by Van der Voo et al. (1997) and Weil et al. (2000, 2001). Originally, the age of the 'B' component magnetization was bracketed by inspection of corrected 'B' component inclinations with available paleomagnetic data from late Paleozoic magnetizations for stable Iberia (e.g., Malod and Mauffret 1990; Van der Voo 1993; Parés et al. 1994) and by estimation of the timing of arc-parallel folding inferred from syntectonic sediments (e.g., Julivert 1971; Marcos and Pulgar 1982; Martínez García 1991; Pérez-Estaún et al. 1994). Deformation of syntectonic deposits from isolated thrust wedges constrains the end of the diachronous arc-parallel thrusting and folding to between the Moscovian and Kasimovian within the CAA (ca. 305 Ma.) (e.g., Alonso 1987; Pérez-Estaún et al. 1988). Following Weil et al. (2010a, b), the 'B' component magnetization is herein assumed to be Kasimovian in age, which matches both the time constraints of folding, and lies within the predicted palaeo-latitudes for Iberia for the late Carboniferous.

Discussion

Fold tests performed on both outcrop-scale and km-scale folds within the Esla Unit constrain the age of magnetization acquisition to after initial D1 folding and concomitant thrust emplacement, but prior to late-stage D2 thrust sheet reactivation and rotation associated with oroclinal buckling of the Cantabrian–Asturian Arc (Fig. 7). Hysteresis properties and demagnetization behavior of the sampled Devonian carbonates are consistent with a 'B'

magnetization, acquired in the Kasimovian at ca. 305 Ma (Van der Voo et al. 1997; Weil et al. 2000, 2010a, b; Weil and Van der Voo 2002b) and is in agreement with independent structural constraints (Pastor-Galán et al. 2011). Consequently, any site mean direction that today is subparallel to the reference 'B' direction represents an area that experienced no significant cumulative rotation subsequent to magnetization acquisition. In contrast, a site mean direction that deviates from the reference direction indicates an area that has undergone appreciable cumulative vertical-axis rotation, which is interpreted to be associated with late-stage north–south compression (in present-day coordinates) and thrust sheet rotation (Fig. 6).

The different tectonic units that comprise the CAA are defined by their lithologic and structural styles (Fig. 1b). Individual tectonic units, depending on their mechanical stratigraphy and geographic position in the overall arc (e.g., hinge zone vs. arc limb), had varying structural responses to the two main deformation phases that formed the CAA. As a result of the strong interactions of tectonic units during protracted deformation, it is important to establish a consistent regional kinematic model that takes advantage of available data from all adjacent tectonic units and incorporates how and when these units affected each other. Of particular relevance to the development of the Esla Unit are the two main units to the north (the Ponga and Picos de Europa units in the hinge zone of the arc) and the southern arm units of the Fold-and-Nappe province to the west (particularly the Sobia-Bodón and Somiedo-Correcillas units) (Fig. 1b).

The Ponga Unit lies in the inner-hinge of the arc (previous structural studies: Julivert 1960; Álvarez-Marrón and Pérez-Estaún 1988; Julivert and Arboleya 1984; Alvarez-Marrón 1995) and is characterized by a highly sinuous map pattern. The structures in the Ponga Unit are dominated by twofold sets that produced complex cross-fold interference patterns (Álvarez- Marrón and Pérez-Estaún 1988; Julivert and Arboleya 1984; Weil 2006). The larger arc-parallel map-scale folds were formed as fault-bend folds of hanging-wall, west-dipping panels translated over frontal and lateral ramps (Álvarez-Marrón and Pérez-Estaún 1988; Julivert and Arboleya 1984). Deformation in the Ponga Unit is dominated by a series of stacked thrusts of varying thicknesses whose deformation history is strongly influenced by their position in the core of the arc, which due to space problems in the foreland during secondary north–south shortening (Rodríguez Fernández and Heredia 1987), caused large-scale buckling, conical folding of the preexisting north–south trending structures, reactivation of lateral ramps, and formation of steep-axis interference folds at thrust culminations (Álvarez- Marrón and Pérez-Estaún 1988; Pérez-Estaún et al. 1988; Weil 2006; Merino-Tomé et al. 2009).

Directly east of the Ponga Unit is the Picos de Europa Unit (Fig. 1b), which is primarily composed of thick Carboniferous limestone sequences that are cut by numerous E-W trending imbricate thrust sheets emplaced toward the south (Marquinez 1978; Pérez-Estaún et al. 1988; Merino-Tomé et al. 2009). This late-stage compression resulted in $>150 \pm 15$ km of crustal shortening (Merino-Tomé et al. 2009). Unlike the Ponga Unit, the Picos de Europe Unit has very few exposed folds and a near absence of secondary superposed structures related to oroclinal bending (Pérez-Estaún et al. 1988; Weil 2006). The relatively simple structural architecture of the Picos de Europe Unit compared to units further west is due to the near absence of D1 deformation, which is a consequence of the unit's inboard position relative to the deforming foreland to the west. The southward-directed imbricate system accounts for a significant amount of N–S shortening, which was required in the hinge zone of the arc due to crustal buckling during D2 deformation. The Moscovian to Gzhelian age of deformation in the Picos de Europa Unit is constrained by occurrences of well-dated synorogenic deposits (Merino-Tomé et al. 2009). Although no paleomagnetic study has been published from the Picos de Europa Unit, little to no large rotations are expected given the present-day geometry and inferred kinematics of the imbricate system (Merino-Tomé et al. 2009).

For the Esla Nappe, localized rotations are observed with a close association to arc-parallel thrusts, suggesting thrust reactivation as the underlying Corniero Nappe was emplaced in an arc-parallel orientation during D2 deformation. However, a consistent pattern of counterclockwise rotation is not observed in the interior Esla Nappe, where in situ paleomagnetic declinations are closer to the regional reference direction, and in some cases record minor clockwise rotations (Fig. 6). This lack of significant rotations in the eastern exposure of the Esla Nappe and the Corniero Nappe exposed in the Valdoré Window is supported by the roughly north–south present-day trend of the main structural features at these localities. Thus, it is unlikely that the Esla Unit underwent simple counterclockwise thrust sheet rotation, as proposed for the larger Somiedo-Correcillas and Sobia-Bodón units to the west (Weil et al. 2001). More likely, the western exposures of the Esla Unit experienced reactivation and modification along the Porma Fault resulting in significant, but localized rotations, whereas the eastern exposure of the Esla Unit likely translated northward during D2 deformation, resulting in interference folds being superimposed on existing D1 structures (e.g., formation of the present-day sinuous axial trace of the Peña Quebrada Synform [originally observed by Alonso (1987)].

In order to develop a feasible working kinematic model, the structures of the Esla Unit are restored to their D1 geometry. Due to the complex interaction of thrusts and superimposed-folding in the Esla Unit, standard unfolding techniques cannot be used to restore bedding to its orientation at the time of remanence acquisition (MacDonald 1980; Pueyo et al. 2003). Because of the aforementioned reasons, each of the studied sites was evaluated separately in the context of local and regional fold axis orientations to determine the best possible sequence of corrections to restore structures to their post-D1 configuration. Restoration of individual sites was attained by calculating the best-fit deformation axes to rotate in situ magnetization vectors back to the reference 'B' magnetization (see details of method in: Bates 1989; Setiabudidaya et al. 1994; Weil et al. 2000; Weil 2006). By definition, no rotation about the axis of the reference magnetization (south–southeasterly and shallow) can be detected by this type of analysis. Using the calculated deformation axes, the regional structural trends of the Esla Unit are restored to their configuration at the time of magnetization acquisition (Figs. 8b, c).

Restoration of paleomagnetic site means, and their associated site mean strikes, results in a much simpler and uniform NNW-SSE trending fold train with near-horizontal fold axes and steep axial surfaces (Fig. 8b, c). This geometry is very similar to the restored post-D1 geometry of large fold domains within the hinge zone of the outer Fold-and-Nappe province (Weil et al. 2000, 2001) as well as the frontal thrusts of the Ponga Unit (Weil 2006).

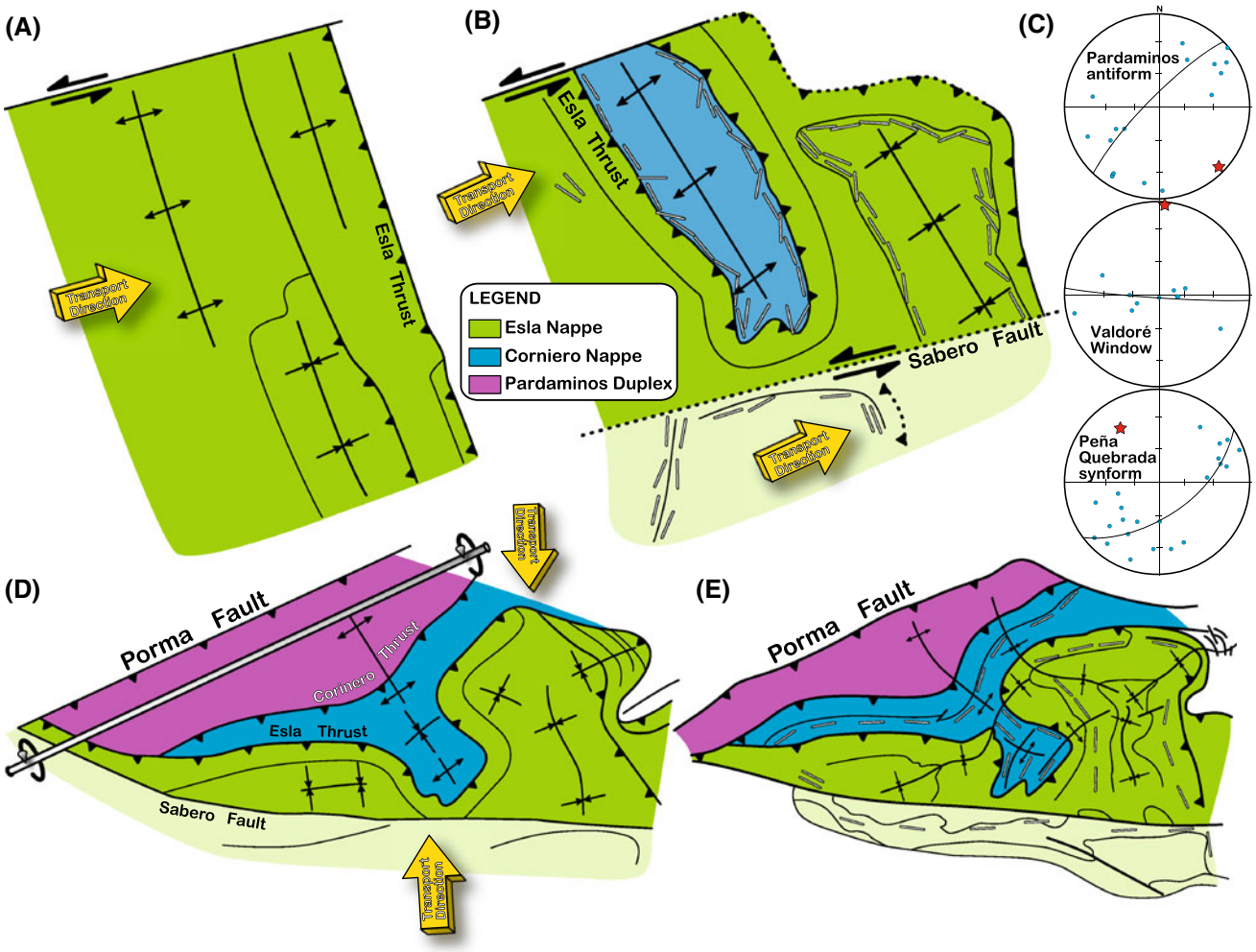

Fig. 8 Representative evolution of Esla Unit outcrop configuration based on restored bedding orientation calculations from this study. **a** Syn-D1 folding and faulting associated with emplacement of the Esla Nappe. **b** Post-D1 restoration with restored individual site means strikes highlighted by *open lines*. **c** Equal area stereonet plots of poles of restored bedding for the three main fold structures (Pardaminos Antiform, Valdoré Window, and the Peña Quebrada Synform). *Great circles* represent best-fit planes to restored bedding, and *red stars* represents best-fit fold axes. **d** Syn-D2 restoration highlighting reactivation of the Porma Fault as a reverse fault, and rotation of the western section of the Esla Unit. **e** Simplified present-day geometry of the Esla Unit with in situ measured site mean strikes plotted. Schematic restoration stages modified after Alonso (1987)

Figure 8a schematically represents the initial outcrop pattern during ENE-directed transport and D1 emplacement of the Esla Nappe and the concomitant formation of hanging-wall folds. Figure 8b shows the post-D1 outcrop pattern of the Esla Unit structural stack—including the effects of the emplacement of the Corniero and Valbuena nappes and the out-of-sequence Pardaminos, Primajas and Pico Jano duplexes at depth. This post-D1 restoration results in structural traces with both NNW-SSE and WSW-ENE trending segments, consistent with the existence of frontal and lateral/oblique footwall-ramp-related fault-bend folds formed during initial D1 thrusting of the Esla Unit (e.g., the Agua Salio Synform, and the WSW-ENE structures south of the Sabero Fault) (Alonso 1987). Such restored patterns suggests that some of the present-day changes in strike in the Esla Unit are not the product of extensive vertical-axis rotation, but are due instead to multiple horizontal-axis rotations that produced corner folds at the intersection of oblique/lateral and frontal ramp surfaces. Thus, depending on whether a site is located above an oblique/lateral ramp or a modified reactivated frontal ramp dictates whether an area is not affected or affected, respectively, by vertical-axis rotations during D2 deformation.

Figure 8c, d highlight thrust sheet modification during D2 north–south shortening. Importantly, the Porma Fault, which started as a transport parallel tear fault during D1 deformation, was reactivated as a reverse fault during D2 shortening (Alonso 1987; Alonso et al. 2009). This reactivation resulted in substantial NE-SW horizontal-axis rotation of the entire Esla Unit thrust stack due to motion along the now reverse Porma Fault system. This northward translation, and subsequent rotation, resulted in the near profile map-view perspective of the Esla Unit nappe-stack seen today (Alonso 1987). Such a perspective makes visualization of vertical-axis rotations challenging, as the current sinuous outcrop trace of the Corniero Nappe is actually an apparent profile-view of an original D1 fold structure (i.e., an apparent down-plunge view of a fold in map view), which was modified during D2 reactivation. This is opposed to the observed systematic vertical-axis rotation of thrust sheets documented in the outer Fold-and-Nappe province of folds with steep upright axial surfaces (e.g., the Lagos del Valle Syncline of Van der Voo et Al. 1997 and the Proaza Antiform of Weil et al. 2000). Figure 8D shows the simplified present-day geometry of the Esla Unit (measured site mean bedding strikes are represented by white lines, see Table 1).

Conclusions

Based on the presented palinspastic restoration of the Esla Unit, considerable modification of D1 lateral and oblique ramp folds, and secondary rotation of D1 frontal ramp folds occurred during late-stage oroclinal bending (Fig. 8). Consequently, the present-day sinuosity of the Esla Unit is the consequence of both secondary rotation of originally linear features, and the secondary modification and tightening of originally curvilinear features (e.g., the hanging-wall lateral/oblique structures in the Esla and Corniero thrust sheets). These results are consistent with previously documented thrust sheet reactivation in the outer Fold-and-

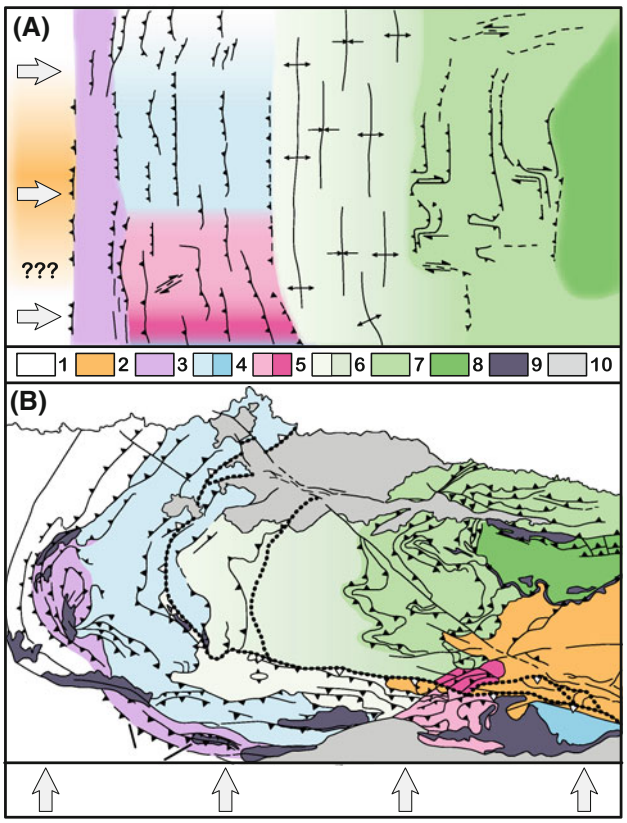

Fig. 9 Cartoon map of palinspastically restored Cantabrian–Asturian Arc showing **a** the general configuration after initial east–west (in present-day coordinates) compression (D1 deformation phase). Orientations of major thrusts are inferred from this study for the Esla Unit, from Weil (2006) for the Ponga Unit, and from Weil et al. (2000, 2001) for the outer Fold-and-Nappe units. *Block arrows* represent the schematic orientation of the ancient stress field during deformation. Fill patterns represent different tectonic units of the Cantabrian–Asturian Arc as depicted in Fig. 1b: (*1*) West Asturian-Leonese; (*2*) Pisuerga-Carrión; (*3*) Narcea Antiform; (*4*) Somiedo/Correcillas-Valsurbio; (*5*) Esla-Lois-Cigüera; (*6*) Sobia/Bodón-Central Coal Basin; (*7*) Ponga; (*8*) Picos de Europa; (*9*) Unconformable Upper Carboniferous rocks; (*10*) Mesozoic and Tertiary cover. **b** Present-day configuration of Cantabrian–Asturian Arc after oroclinal bending, which resulted in counterclockwise rotation of the southern limb Pisuerga-Carrión, Narcea Antiform, and Somiedo/Correcillas-Valsurbio units, clockwise rotation of the northern limb and buckling, superposed and radial folding, and thrust reactivation in the central core and hinge of the arc (mainly the Sobia/Bodón-Central Coal Basin, Ponga and Picos de Europa units) as well as the southeastern Esla-Lois-Cigüera units

Nappe province in which nearly all present-day curvature is secondary and resulted from buckling and conical folding of an originally more linear fold-thrust belt (Van der Voo et al. 1997; Weil et al. 2000, 2001; Pastor-Galán et al. 2012), and the Ponga Unit (Weil 2006) where map view sinuosity is due to both secondary rotation and complex thrust reactivation creating interference folds.

Paleomagnetic observations from throughout the CAA, including the present results from the Esla Unit, indicate that the Variscan tectonic history in the CAA involved at least two temporally discrete deformation phases. The first deformation phase resulted in thrusting and folding related to west-to-east tectonic transport (in present-day coordinates), which migrated in time from west to east and lasted into the Kasimovian (Fig. 9a). Thrusting during this initial phase resulted in locally complex footwall geometries characterized by frontal and oblique/lateral ramps—particularly in the Esla and Ponga units. D1 folding was followed by the acquisition of the 'B' magnetization and, subsequently, in the latest Carboniferous to earliest Permian, by D2 deformation. This late Variscan phase of deformation buckled originally linear, north–south (in present-day coordinates) trending thrusts and hanging-wall folds (mainly by conical folding in the hinge zones of the arc), and modified drape folds associated with D1 frontal/lateral/oblique ramp intersections. Thrust sheet modification was accommodated by reactivation of lateral/oblique ramps as frontal ramps (e.g., the Porma Fault), reactivation of frontal ramps as oblique ramps, and overall tightening of D1 folds, often by conical folding of existing D1 arc-parallel fold limbs (Figs. 8, 9). These structural modifications were necessary for accommodating north–south shortening associated with oroclinal bending (Fig. 9). The ultimate change from east–west to north–south compression near the Carboniferous/Permian boundary in the Cantabrian–Asturian Arc region was likely the result of the final collision of the North African margin of Gondwana with southwestern Europe during the last stages of Pangea amalgamation (Weil et al. 2001, 2010a, b; Gutiérrez-Alonso et al. 2008). Within this broader scenario, local, north–south compression in the Esla Unit was driven by the southward thrusting of the Picos de Europa thrust package late in the evolution of the CAA (Merino-Tomé et al. 2009).

Acknowledgments Funding for A.B.W. and G.G-A. came from Spanish Education and Science Ministry Project Grant CGL2009-1367 (O.D.R.E. II). The Institute for Rock Magnetism (IRM) at the University of Minnesota is thanked for giving A.B.W. time for hysteresis analysis. The IRM is funded by the Instruments and Facilities Program, Earth Sciences Division, National Science Foundation, and the W. M. Keck Foundation. A special thanks to several field assistance during the years of sampling—John W. Geissman (UT Dallas), Nicholas Lea Bruno, Jessica Shaw and Daniel Pastor-Galán. D. Wicks received summer research funding from the Bryn Mawr College Summer Science Research Program. This project was carried out in partial fulfillment of D. Wicks's undergraduate thesis at Bryn Mawr College. Special thanks are given to Martin Keller, an anonymous reviewer, and the editorial staff at the International Journal of Earth Sciences for their helpful comments, which improved the readability and accessibility of the manuscript.

References

Allerton S (1998) Geometry and kinematics of vertical-axis rotations in fold and thrust belts. Tectonophysics 299:15–30

Alonso JL (1987) Sequences of thrusts and displacement transfer in the superposed duplexes of the Esla Nappe region (Cantabrian Zone, NW Spain). J Struct Geol 9:969–983

Alonso JL (1989) Fold reactivation involving angular unconformable sequences—theoretical-analysis and natural examples from the Cantabrian Zone (northwest Spain). Tectonophysics 170: 57–77

Alonso JL, Marcos A, Suárez A (2009) Paleogeographic inversion resulting from large out of sequence breaching thrusts: the León Fault (Cantabrian Zone, NW Iberia). A new picture of the external Variscan Thrust Belt in the Ibero-Armorican Arc. Geologica Acta 7:451–473

Álvarez- Marrón J, Pérez-Estaún A (1988) Thin-skinned tectonics in the Ponga Region (Cantabria Zone, NW Spain). Geol Rundsch 77:539–550

Alvarez-Marrón J (1995) Three-dimensional geometry and interference of fault-bend folds: examples from the Ponga Unit, Variscan Belt, NW Spain. J Struct Geol 17:549–560

Aramburu C, Méndez-Bedia I, Arbizu M (2002) The lower paleozoic in the cantabrian zone (Cantabrian Mountains, NW Spain). In: García-López S, Bastida F (eds) Paleozoic conodonts from north Spain. Cuadernos del Museo Geominero 1:35–49

Arboleya ML (1981) La estructura del Manto del Esla (Cordillera Cantábrica, León). Boletín Geológico y Minero XCII-I:19–40

Bates MP (1989) Palaeomagnetic evidence for rotations and deformation in the Nogueras Zone, Central Southern Pyrenees, Spain. J Geol Soc Lond 146:459–476

Bonhommet N, Cobbold PR, Perroud H, Richardson A (1981) Paleomagnetism and cross-folding in a key area of the Asturian Arc (Spain). J Geophys Res 86:1873–1887

Butler RWH (1982) The terminology of structures in thrust belts. J Struct Geol 4:239–245

Channell JET, Lowrie W, Medizza F, Alvarez W (1978) Palaeomagnetism and Tectonics in Umbria, Italy. Earth Planet Sci Lett 39:199–210

Colmenero JR, Suárez-Ruiz I, Fernández-Suárez J, Barba P, Lorens T (2008) Genesis and rank distribution of Upper Carboniferous coal basins in the Cantabrian Mountains, Northern Spain. Int J Coal Geol 76:3187–3204

Day R, Fuller M, Schmidt VA (1977) Hysteresis properties of titanomagnetites: grain-size and compositional dependence. Phys Earth Planet Int 13:260–267

De Sitter LU (1965) The Hercynian Cantabrian orogen. Memoiria Geopaleontologia Università Ferrara 1:211–225

Demarest H (1983) Error analysis for the determination of tectonic rotation from paleomagnetic data. J Geophys Res 88:148–227

Eldredge S, Van der Voo R (1988) Paleomagnetic study of thrust sheet rotations in the Helena and Wyoming salients of the Northern Rocky Mountains. In: Schmidt CJ (ed) Interaction of the rocky mountain foreland and the cordilleran thrust belt. Memoir Geol Soc Am 171:319–332

Eldredge S, Bachtadse V, Van der Voo R (1985) Paleomagnetism and the orocline hypothesis. Tectonophysics 119:153–179

Fernández LP, Fernández-Martínez EM, García-Ramos JC, Méndez-Bedia I, Soto F (1997) A sequential approach to the study of reefal facies in the Candás and Portilla Formations (Middle Devonian) of the Cantabrian Zone (NW Spain). Boletín de la Real Sociedad Española de Historia Natural (Geología) 92:23–33

Fisher R (1953) Dispersion on a sphere: proceedings of the royal society of London. Ser A Math Phys Sci 217:295–305

Franke W (2000) The mid-European segment of the Variscides: tectonostratigraphic units, terrane boundaries and plate tectonic evolution. In: Franke W, Haak V, Oncken O, Tanner D (eds) Orogenic processes: quantification and modeling in the Variscan Belt, vol 179. The Geological Society of London, Special Publication, pp 35–61

Franke W, Matte P, Tait J (2005) Variscan orogeny: Europe. Elsevier Ltd., Amsterdam, pp 75–85

García-Alcalde JL (1995) L'evolution paléogéographique pré-varisque de la Zone Cantabrique septentrional (Espagne). Revista Española de Paleontología 10:9–29

García-López S (2002) A stratigraphic overview of the Cantabrian Devonian (NW Spain). In: García-López S, Bastida F (eds) Paleozoic conodonts from north Spain. Cuadernos del Museo Geominero 1:51–59

García-Ramos JC, Colmenero JR (1981) Evolución sedimentaria y paleogeográfica durante el Devónico en la Cordillera Cantábrica. Real Acad de Ciencias Exactas Físicas y Nat 2:61–76

Gasparrini M, Bakker RJ, Bechstädt T, Boni M (2003) Hot dolomites in a Variscan foreland belt: hydrothermal flow in the Cantabrian Zone (NW Spain). J Geochem Explor 78–79:501–507

Gasparrini M, Bechstädt T, Boni M (2006) Massive hydrothermal dolomite in the southwestern Cantabrian Zone (Spain) and its relation to the late Variscan evolution. Mar Pet Geol 23:543–568

Grubbs KL, Van der Voo R (1976) Structural deformation of the Idaho-Wyoming overthrust belt (USA), as determined by Triassic paleomagnetism. Tectonophysics 33:321–336

Gutiérrez-Alonso G, Fernandez-Suarez J, Weil AB, Murphy JB, Nance RD, Corfu F, Johnston ST (2008) Self-subduction of the Pangaean global plate. Nat Geosci 1:549–553

Hindle H, Burkhard M (1999) Strain, displacement and rotation associated with the formation of curvature on fold belts; the example of the Jura arc. J Struct Geol 21:1089–1101

Hirt AM, Lowrie W, Julivert M, Arboleya ML (1992) Paleomagnetic results in support of a model for the origin of the Asturian Arc. Tectonophysics 213:321–339

Hoffman KA, Day R (1978) Separation of multi-component NRM: a general method. Earth Planet Sci Lett 40:433–438

Hofmann MH, Keller M (2006) Sequence stratigraphy and carbonate platform organization of the Devonian Santa Lucia Formation, Cantabrian Mountains, NW-Spain. Facies 52:149–167

Irving E, Opdyke ND (1965) The paleomagnetism of the Bloomsburg redbeds and its possible application to the tectonic history of the Appalachians. Geophys J R Astron Soc 9:153–167

Jackson M, Sun WW, Craddock JP (1992) The rock magnetic fingerprint of chemical remagnetization in midcontinental Paleozoic carbonates. Geophys Res Lett 19:781–784

Julivert M (1960) Estudia geologico de la cuenca de Beleno. Valles altos del Sella, Ponga, Nalon y Esla de la Cordillera Cantabria. Boletin del Instituto Geológico y Minero de España 71:1–346

Julivert M (1971) Décollement tectonics in the Hercynian Cordillera of NW Spain. Am J Sci 270:1–29

Julivert M, Arboleya ML (1984) A geometrical and kinematical approach to the nappe structure in an arcuate fold belt—the Cantabrian Nappes (Hercynian Chain, Nw Spain). J Struct Geol 6:499–519

Julivert M, Marcos A (1973) Superimposed folding under flexural conditions in the Cantabrian Zone (Hercynian Cordillera, northwest Spain). Am J Sci 271:353–375

Keller M (1997) Evolution and sequence stratigraphy of an early Devonian carbonate ramp, Cantabrian Mountains, Northern Spain. J Sediment Res 67:638–652

Keller M, Bahlburg H, Reuther CD, Weh A (2007) Flexural to broken foreland basin evolution as a result of Variscan collisional events in northwestern Spain. In: Hatcher RD, Carlson MP, McBride JH, Catalan JRM (eds) 4-D framework of continental crust, vol 200. Geological Society of America, Boulder, pp 489–510

Keller M, Bahlburg H, Reuther C-D (2008) The transition from passive to active margin sedimentation in the Cantabrian Mountains, Northern Spain: Devonian or Carboniferous? Tectonophysics 461:414–427

Kent D (1988) Further paleomagnetic evidence for oroclinal rotation in the central folded appalachians from the Bloomsburg and the Mauch Chunk formations. Tectonics 7:749–759

Kent D, Opdyke ND (1985) Multicomponent magnetization from the Mississippian Mauch Chunk formation of the central Appalachians and their tectonic implications. J Geophys Res 90:5371–5383

Kirschvink JL (1980) The least-squares line and plane and the analysis of paleomagnetic data. Geophys J Roy Astron Soc 62:699–718

Kollmeier JM, van der Pluijm BA, Van der Voo R (2000) Analysis of Variscan dynamics; early bending of the Cantabria-Asturias Arc, Northern Spain. Earth Planet Sci Lett 181:203–216

Kotasek J, Krs M (1965) Palaeomagnetic study of tectonic rotation in the Carpathian mountains of Czechoslovakia. Palaeogeogr Palaeoclimatol Palaeoecol 1:39–49

Lowrie W, Hirt AM (1986) Paleomagnetism in Arcuate Mountain Belts. In: The origin of arcs, Developments in Geotectonics 21. Elsevier, Amsterdam, pp 141–158

MacDonald WD (1980) Net tectonic rotation, apparent tectonic rotation, and the structural tilt correction in paleomagnetic studies, in Norman Watkins memorial. J Geophys Res 85:3659–3669

Malod JA, Mauffret A (1990) Iberian plate motions during the Mesozoic. Tectonophysics 184:261–278

Marcos A, Pulgar JA (1982) An approach to the tectonostratigraphic evolution of the Cantabrian foreland thrust and fold belt, Hercynian Cordillera of NW Spain. Neues Jahrbuchlür Geologie und Palantologie Abhandlungen 163:256–260

Marquinez J (1978) Estudio geológico del sector SE de los Picos de Europa (Cordillera Cantábrica, NW de España). Trabajos de Geología Universidad de Oviedo 10:295–315

Marshak S (1988) Kinematics of orocline and arc formation in thin skinned orogens. Tectonics 7:73–86

Marshak S (2004) Arcs, oroclines, salients, and syntaxes. The origin of map-view curvature in fold-thrust belts. In McClay KR (ed) Thrust tectonics and petroleum systems. Am Assoc Petrol Geol Mem 82:131–156

Marshak S, Wilkerson MS, Hsui AT (1992) Generation of curved fold-thrust belts: insights from simple physical and analytical models. In: McClay K (ed) Thrust tectonics. Chapman and Hall, London, pp 83–92

Martínez García E (1991) Hercynian synorogenic and postorogenic successions in the Cantabrian and Palentian zones, NW Spain. Comparison with other western European occurrences. Giorn Geol 53:209–228

Martínez-Catalán JR (2011) Are the oroclines of the Variscan belt related to late Variscan strike-slip tectonics? Terra Nova 23:241–247

Martínez-Catalán JR, Arenas R, Díaz García F, Gómez-Barreiro J, González Cuadra P, Abati J, Castiñeiras P, Fernández-Suárez J, Sánchez Martínez S, Andonaegui P, Gónzalez Clavijo E, Díez Montes A, Rubio Pascual FJ, Valle Aguado B (2007) Space and time in the tectonic evolution of the northwestern Iberian Massif: implications for the Variscan belt. In: Hatcher Jr RD, Carlson MP, McBride JH, Mart+Ànez Catal+Ún JR (eds) 4-D framework

of continental, vol 200. Geological Society of America, Denver, pp 403–423
Matte P (1986) Tectonics and plate tectonics model for the Variscan belt of Europe. Tectonophysics 126:329–374
Matte P (1991) Accretionary history and crustal evolution of the Variscan belt in Western Europe. Tectonophysics 196:309–337
McCabe C, Channell JET (1994) Late Paleozoic remagnetization in limestones of the Craven Basin (northern England) and the rock magnetic fingerprint of remagnetized sedimentary carbonates. J Geophys Res 99:4603–4612
McCaig AM, McClelland E (1992) Palaeomagnetic techniques applied to thrust belts. In: McClay K (ed) Thrust tectonics. Chapman and Hall, London, pp 209–216
McElhinny MW (1964) Statistical significance of the fold test in paleomagnetism. R Astron Soc Geophys J 8:338–340
Méndez-Bedia I (1976) Biofacies y litofacies de la formación Moniello-Santa Lucía (Devónico de la Cordillera Cantábrica, NW de España). Trabajos de Geología Universidad de Oviedo 9:93 pp
Méndez-Bedia I, Soto F, Fernández Martínez E (1994) Devonian reef types in the Cantabrian Mountains (NW Spain) and their faunal composition. Courier Forschungsinstitut Senckenberg 172:161–183
Merino-Tomé OA, Bahamonde JR, Colmenero JR, Heredia N, Villa E, Farias P (2009) Emplacement of the Cuera and Picos de Europa imbricate system at the core of the Iberian-Armorican arc (Cantabrian zone, north Spain): new precisions concerning the timing of arc closure. Geol Soc Am Bull 121:729–751
Miller JD, Kent DV (1986a) Paleomagnetic of the Upper Devonian catskill formation from the southern limb of the Pennsylvania Salient: possible evidence of oroclinal rotation. Geophys Res Lett 13:1173–1176
Miller JD, Kent DV (1986b) Synfolding and prefolding magnetizations in the upper Devonian Catskill formation of eastern Pennsylvania: implication for the tectonic history of Acadia. J Geophys Res 91:12791–12803
Molina-Garza RS, Zijderveld JDA (1996) Paleomagnetism of Paleozoic strata, Brabant and Ardennes Massifs, Belgium: implications of prefolding and postfolding Late Carboniferous secondary magnetizations for European polar wander. J Geophys Res 101:15799–15818
Muttoni G, Argnani A, Kent DV, Abrahamsen N, Cibin U (1998) Paleomagnetic evidence for Neogene tectonic rotations in the northern Apennines, Italy. Earth Planet Sci Lett 154:25–40
Muttoni G, Lanci L, Argnani A, Hirt AM, Cibin U, Abrahamsen N, Lowrie W (2000) Paleomagnetic evidence for a Neogene two-phase counterclockwise tectonic rotation in the Northern Apennines (Italy). Tectonophysics 326:241–253
Parés JM, Van der Voo R, Stamatakos J, Pérez-Estaún A (1994) Remagnetizations and postfolding oroclinal rotations in the Cantabrian/Asturian arc, Northern Spain. Tectonics 13:1461–1471
Pastor-Galán D, Gutiérrez-Alonso G, Meere PA, Mulchrone KF (2009) Factors affecting finite strain estimation in low-grade, low-strain clastic rocks. J Struct Geol 31:1586–1596
Pastor-Galán D, Gutierréz-Alonso G, Weil AB (2011) Orocline timing through joint analysis: Insights from the Ibero-Armorican Arc. Tectonophysics 507:31–46
Pastor-Galán D, Gutiérrez-Alonso G, Mulchrone KF, Huerta P (2012) Conical folding in the core of an orocline. A geometric analysis from the Cantabrian Arc (Variscan Belt of NW Iberia). J Struct Geol. http://dx.doi.org/10.1016/j.jsg.2012.02.010
Pérez-Estaún A, Bastida F, Alonso JL, Marquinez J, Aller J, Alvarezmarron J, Marcos A, Pulgar JA (1988) A thin-skinned tectonics model for an arcuate fold and thrust belt—the Cantabrian Zone (Variscan Ibero-Armorican Arc). Tectonics 7:517–537
Pérez-Estaún A, Martínez Catalán JR, Bastida F (1991) Crustal thickening and deformation sequence in the footwall to the suture of the Variscan Belt of northwest Spain. Tectonophysics 191:243–253
Pérez-Estaún A, Pulgar JA, Banda E, Álvarez-Marón J (1994) Crustal structure of the external Variscides in NW Spain from deep seismic reflection profiling. Tectonophysics 232:91–118
Perroud H (1986) Paleomagnetic evidence for tectonic rotations in the Variscan Mountain Belt. Tectonics 5:205–214
Pueyo EL, Pocovi A, Pares JM, Millan H, Larrasoana JC (2003) Thrust ramp geometry and spurious rotations of paleomagnetic vectors. Studia Geophys Geodaetica 47:331–358
Pueyo EL, Pocoví A, Millán H, Sussman AJ (2004) Map-view models for correcting and calculating shortening estimates in rotated thrust fronts using paleomagnetic data. Geol Soc Am Spec Pap 383:57–71
Pueyo EL, Mauritsch HJ, Gawlick HJ, Scholger R, Frisch W (2007) New evidence for block and thrust sheet rotations in the Central Northern Calcareous Alps deduced from two pervasive remagnetization events. Tectonics 26: TC5011, 25 pp
Reijers TJA (1980) Sedimentary mechanisms in Spanish Devonian Carbonates. Geol Mijnbouw 59:87–96
Reijers TJA (1985) Devonian basin-fill histories of the Spanish Cantabrian Mountains and the Belgian Ardennes; a comparison. Geol Mijnbouw 64:41–62
Ribeiro A, Munha J, Dias R, Mateus A, Pereira E, Ribeiro L, Fonseca P, Araujo A, Oliveira T, Romao J, Chamine H, Coke C, Pedro J (2007) Geodynamic evolution of the SW Europe Variscides. Tectonics 26:1–24. doi:10.1029/2006TC002058
Ries AC, Richardson A, Shackleton RM (1980) Rotation of the Iberian arc: paleomagnetic results from north Spain. Earth Planet Sci Lett 50:301–310
Rodríguez Fernández LR, Heredia N (1987) La estratigraña del Carbonífero y la estructura de la unidad del Pisuerga-Carrión. NO de España. Cuadernos Laboratorio Xeolóxico de Laxe 12:207–229
Rodríguez J, Cosca MA, Gil Ibarguchi JL, Dallmeyer RD (2003) Strain partitioning and preservation of 40Ar/39Ar ages during Variscan exhumation of a subducted crust (Malpica -Tui complex, NW Spain). Lithos 70:111–139
Santos Zalduegui JF, Scharer U, Oil Ibarguchi JI (1995) Isotope constraints on the age and origin of magmatism and metamorphism in the Malpica-Tuy allochthon, Galicia, NW-Spain. Chem Geol 121:91–103
Schwartz SY, Van der Voo R (1984) Paleomagnetic study of thrust sheet rotation during foreland impingement in the Wyoming-Idaho Overthrust Belt. J Geophys Res 89:10071–10086
Setiabudidaya DJ, Piper DA, Shaw J (1994) Paleomagnetism of the (Early Devonian) lower old red sandstones of south Whales: implications to Variscan overprinting and differential rotations. Tectonophysics 231:257–280
Stewart SA (1995a) Paleomagnetic analysis of fold kinematics and implications for geological models of the Cantabrian/Asturian Arc North Spain. J Geophys Res Solid Earth 100:20079–20094
Stewart SA (1995b) Paleomagnetic analysis of plunging fold structures—errors and a simple fold test. Earth Planet Sci Lett 130:57–67
Tauxe L (1998) Paleomagnetic principles and practice. Modern approaches in geophysics 17. Kluwer Academic Publishers, London
Tauxe L, Watson GS (1994) The fold test: an eigen analysis approach. Earth Planet Sci Lett 122:331–341
Tauxe L, Mullender TAT, Pick A (1996) Potbellies, wasp-waists, and superparamagnetism in magnetic hysteresis. J Geophys Res 101:571–583

Thominski HP, Wohlenberg J, Bleil U (1993) The remagnetization of Devono-Carboniferous sediments from the Ardenno-Rhenish Massif. Tectonophysics 225:411–431

Tornos F, Saphiro BF (2000) The geology and isotope geochemistry of the talc deposits of Puebla de Lillo (Cantabrian Zone, Northern Spain). Econ Geol 95:1277–1296

Van der Voo R (1993) Paleomagnetism of the Atlantic, Tethys and Iapetus Oceans. Cambridge University Press, New York

Van der Voo R (2004) Paleomagnetism, oroclines, and growth of the continental crust. GSA Today 14:4–9

Van der Voo R, Channell JET (1980) Paleomagnetism in Orogenic Belts. Rev Geophys Space Phys 18:455–481

Van der Voo R, Stamatakos JA, Pares JM (1997) Kinematic constraints on thrust-belt curvature from syndeformational magnetizations in the Lagos del Valle Syncline in the Cantabrian Arc, Spain. J Geophys Res Solid Earth 102:10105–10119

Weil AB (2006) Kinematics of orocline tightening in the core of an arc: paleomagnetic analysis of the Ponga Unit, Cantabrian Arc, northern Spain. Tectonics 25:1–23

Weil AB, Sussman A (2004) Classifying curved orogens based on timing relationships between structural development and vertical-axis rotations. Geol Soc Am Spec Pap 383:1–17

Weil AB, Van der Voo R (2002a) The evolution of the paleomagnetic fold test as applied to complex geologic situations, illustrated by a case study from northern Spain. Phys Chem Earth 27:1223–1235

Weil AB, Van der Voo R (2002b) Insights into the mechanism for orogen related carbonate remagnetization from growth of authigenic Fe-oxide: A SEM and rock magnetic study of Devonian carbonates from northern. J Geophys Res 107:2001JB000200

Weil AB, Van der Voo R, van der Pluijm BA, Pares JM (2000) The formation of an orocline by multiphase deformation: a paleomagnetic investigation of the Cantabria-Asturias Arc (northern Spain). J Struct Geol 22:735–756

Weil AB, Van der Voo R, van der Pluijm BA (2001) Oroclinal bending and evidence against the Pangea megashear: the Cantabria-Asturias arc (northern Spain). Geology 29:991–994

Weil AB, Yonkee AW, Sussman AJ (2010a) Reconstructing the kinematic evolution of curved mountain belts: a paleomagnetic study of Triassic red beds from the Wyoming salient, Sevier thrust belt, USA. Geol Soc Am Bull 122:3–23

Weil AB, Gutierrez-Alonso G, Conan J (2010b) New time constraints on lithospheric-scale oroclinal bending of the Ibero-Armorican Arc: a palaeomagnetic study of earliest Permian rocks from Iberia. J Geol Soc 167:127–143

Wotte T (2009) Re-interpretation of a Lower-Middle Cambrian West Gondwanan ramp depositional system: a case study from the Cantabrian Zone (NW Spain). Facies 55:473–487

Yonkee A, Weil AB (2010) Quantifying vertical-axis rotation in curved orogens: integrating multiple data sets with a refined weighted least-squares strike test. Tectonics. doi:10.1029/2008TC002312

Zegers TE, Dekkers MJ, Bailly S (2003) Late Carboniferous to Permian remagnetization of Devonian limestones in the Ardennes: role of temperature, fluids and deformation. J Geophys Res. doi:10.1029/2002JB00221

Zijderveld JDA (1967) AC demagnetization of rocks. Analysis of results. In: Collison DW, Runcorn SK, Creer KM (eds) Methods in Paleomagnetism. Elsevier, New York, pp 254–286